ESA Cloud_cci

Algorithm Theoretical Baseline Document v5.1
Community Cloud retrieval for Climate (CC4CL)

(Applicable to Cloud_cci version 2.0 products)

Issue 5 Revision 1

28/8/2017

Deliverable No.: D-2.1
ESRIN/Contract No.: 4000109870/13/I-NB

Project Coordinator: Dr. Rainer Hollmann
Deutscher Wetterdienst
rainer.hollmann@dwd.de

Technical Officer: Dr. Simon Pinnock
European Space Agency
Simon.Pinnock@esa.int

Document authors: Caroline A. Poulsen[1], Gareth E. Thomas[1], Richard Siddans[1], Adam Povey[2]
Greg McGarragh[2], Cornelia Schuldt[3], Stefan Stapelberg[3], Martin Stengel[3]
and Roy G. Grainger[2]

[1] Space Science and Technology Department, RAL, Chilton, Didcot, OX11 0QX, UK
[2] Atmospheric, Oceanic and Planetary Physics, University of Oxford, Oxford, OX1 3PU, UK
[3] Deutscher Wetterdienst, Frankfurter Str. 135, 63067 Offenbach, Germany

Contents

1 Introduction

This document describes an optimal estimation retrieval scheme for the derivation of the properties of clouds from top-of-atmosphere (TOA) radiances measured by satellite-borne visible-IR radiometers as described in greater detail by Poulsen et al. [2012] and Watts et al. [1998]. The algorithm makes up part of the Community Code for CLimate (CC4CL) retrieval scheme (the other part, known as ORAC, performs aerosol retrievals and is described in Thomas et al. [2010]). CC4CL was originally designed for application to SEVIRI and was subsequently adapted for the ATSR instrument, which was used to produce the GRAPE (Global Retrieval of ATSR cloud Parameters and Evaluation) data set. Within the Cloud_cci framework, the algorithm has been applied to AVHRR and MODIS using the 'heritage' set of channels (i.e. channels equivalent to the 0.67, 0.87, 1.6, 3.7, 11 and 12 μm channels of AVHRR) to produce a long-term climate data record with global coverage. In the text that follows, the description will often refer to AATSR but is equally applicable to instruments with similar channel definitions.

Specific features of this algorithm include:

- A full implementation of the optimal estimation framework described by Rodgers [2000], enabling rigorous error propagation and inclusion of *a priori* knowledge.
- A common retrieval algorithm over both land and ocean, with only the *a priori* constraint on the surface reflectance differing between the two.
- Consistent and simultaneous retrieval of all cloud parameters in the visible and infrared.

2 Retrieval system description

CC4CL consists of three main components: (1) cloud detection (2) cloud typing and (3) the retrieval of cloud properties based on OE technique. These components are described in more detail in the following sections.

2.1 Cloud detection

The cloud mask is based on artificial neural networks (ANNs). Three ANNs were trained: for day (using visible (VIS), near-infrared (NIR) and infrared (IR) information), for night/twilight (using NIR and IR channels), and again for night/twilight with different channel input (IR channels only). The ANNs have been trained based on collocations between AVHRR NOAA-18 measurements and CALIPSO COD data. As a result a pseudo CALIPSO optical depth (ANNCOD) is computed (mimicked) and converted into a 2 bit cloud mask by applying thresholds.

The used ANN's are multilayer perceptrons consisting of 1 input layer, one hidden layer with about 50 neurons and one output layer. The training and test datasets are based on collocated CALIPSO COD data (CAL_LID_L2_05kmCLay-Prov-V3-01, total optical thickness at 532nm) and Cloud_cci AVHRR GAC Level-1C measurements. The Day ANN was trained with VIS and IR data. For consistency, Ch3b (3.7 m) of AVHRR was not included in the Day ANN, because NOAA-17, METOP-A and partly NOAA-16 switch between 1.6μm and 3.7μm during day and night-time. The 2 night ANN's have been trained both with and without the 3.7μm NIR channel information. This avoids the misclassification of very cold clouds and/or surfaces because of very low 3.7μm channel signalto-noise-ratios.

Overall, 12 globally and seasonally representative days in 2008 with best collocations between NOAA-18 and CALIPSO have been chosen as training dataset. Prior to that, all collocated CALIPSO CODs greater 1 have been set to 1. In a final step, a simple viewing-angle correction is applied to the retrieved ANNCOD which tends to increase with increasing viewing-angle. For the generation of the final 2-bit cloud mask, suitable thresholds have been found and applied to the ANNCOD. In the following the most important ANN facts

a summarized.

Trainings dataset:
12 days of 2008 of AVHRR NOAA-18 (DOYs=[15,58,80,117,139, 165,172,194,265,305,320, 355]) collocated to CALIPSO. training algorithm: back-propagation

ANN input data - day:
Ch1 (0.6μm), Ch2 (0.8μm), CH4 (11μm), CH5 (12μm), CH4-CH5, ERA-Interim skin temperature, Land-Sea Mask, Snow-Ice Flag (NISE[1])

ANN input data - night/twilight (NIR+IR):
CH3b (3.7μm), CH4 (11μm), CH5 (12μm), CH4-CH5, CH4-Ch3b, ERA-Interim skin temperature, Land-Sea Mask, Snow-Ice Flag (NISE)

AAN input data - night/twilight (IR):
CH4 (11μm), CH5 (12μm), CH4 CH5, ECMWF-Skin Temperature, Land-SeaMask, Snow-Ice Flag (NISE)

AAN Output Parameter:
a pseudo-CALIPSO-COD (ANNCOD) ranging from 0 to 1. The ANNCOD is set to fill-value if non of the input channels have valid measurements.

Cloud-Mask Thresholds:
Table 1 lists the threshold applied to determine the binary cloud decision from ANNCOD. The thresholds depend on illumination and surface type.

As the ANNs were trained using NOAA-18 AVHRR measurements, a radiances adjustment has been determined for AATSR and MODIS to make them mimic AVHRR. The adjustment includes slopes and offsets based on collocations of AATSR and MODIS-Aqua measurements with NOAA-18 AVHRR. The slope and offset values are listed in Table 2.

Cloud detection uncertatinty :
Based on the training set. The binary results (after applying ANN and thresholds) were compared against the CALIOP cloud mask and detection scores calculated. The scores show a clear dependence on the distance between the ANNCOD and the respective threshold, which allows a approximation of the cloud detection uncertainty on pixel level based on these two values. Figure 1 shows the probability of incorrect cloud mask as a function of normalized ANNCOD-threshold distance.

2.2 Cloud typing (incl. phase determination)

A new cloud typing algorithm has been implemented in the preprocessing to select a cloud phase based on the cloud type it selects:

- The following categories indicate the liquid cloud phase:
  - fog,
  - warm liquid water clouds, and
  - supercooled-mixed-phased clouds.

[1]Near-real-time Ice and Snow Extent (NISE) data set of the National Snow and Ice Data Center

Table 1: Threshold values applied to ANNCOD data for cloud mask classification. Table taken from Sus el al. [2017]

day	night	twilight	land	sea	snow/ice	threshold
x			x			0.2
x			x		x	0.35
x				x		0.1
x				x	x	0.4
	x		x			0.3
	x		x		x	0.35
	x			x		0.2
	x			x	x	0.4
		x	x			0.3
		x	x		x	0.4
		x		x		0.35
		x		x	x	0.4

Table 2: Linear regression coefficients between collocated AVHRR and MODIS/AATSR channels. Table taken from Sus el al. [2017]. WL stands for wavelengths.

CC4CL channel ID	centre WL [mic]	sensor	regression coefficients
1	0.6	MODIS	0.8945 × ch1 + 2.217
		AATSR	0.8542 × ch1
2	0.8	MODIS	0.8336 × ch2 + 1.749
		AATSR	0.7787 × ch2
4	3.7	MODIS	0.9944 × ch4 + 1.152
		AATSR	1.0626 × ch4 - 15.777
5	10.8	MODIS	0.9742 × ch5 + 7.205
		AATSR	0.9793 × ch5 + 5.366
6	12.0	MODIS	0.9676 × ch6 + 8.408
		AATSR	0.9838 × ch6 + 4.255

- The following categories indicate the ice cloud phase:
  - opaque ice clouds/deep convection,
  - non-opaque high ice clouds (e.g. cirrus),
  - cloud overlap[2] (e.g. multiple cloud layers), and
  - probably-opaque ice clouds (e.g. neither 1.6 μm nor 3.7 μm channel is available during night for AVHRR; 12 μm channel is missing during night for AATSR).

Usually, CC4CL performs separate retrievals for each phase and selects the appropriate phase as that with the lowest retrieval cost (eqn. 1). If desired, CC4CL can now process only once assuming the phase identified above.

A detailed description of daytime spectral tests using AVHRR, MODIS and VIIRS observations is given in Pavolonis and Heidinger [2004] and Pavolonis et al. [2005] along with inter-comparison results. The multi-spectral algorithm used in CC4CL is based on the threshold approach described in these papers but can retrieve

[2]Assuming that a scene with cloud overlap consists of a semitransparent ice cloud that overlaps a cloud composed of liquid water droplets [Pavolonis and Heidinger, 2004].

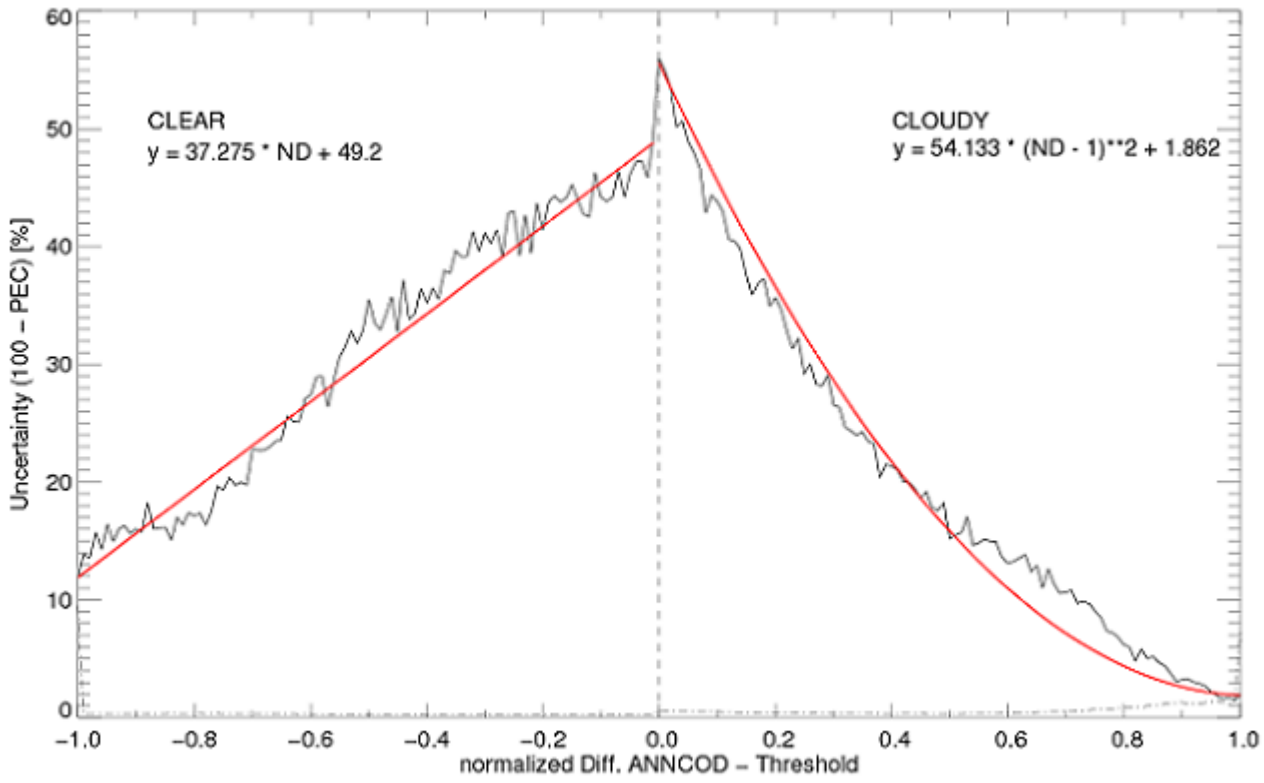

Figure 1: Neural network cloud mask uncertainty. Figure taken from Sus el al. [2017]

in the absence of visible/near-IR measurements (e.g. at night) and includes a new threshold test required for AVHRR and A(A)TSR measurements (i.e. the probably-opaque ice clouds).

To briefly summarize the main features of the algorithm, the cloud type retrieval requires as input satellite imager data at 0.65, 1.6(3a)/3.75(3b), 10.8 and 12 μm. If both 1.6 and 3.75 μm data are available, the 3.75 μm reflectances are used.[3] Pavolonis et al. [2005] have analyzed cloud typing results based on channel 3a or 3b and concluded that both algorithms produce nearly identical results except for certain thin clouds and at cloud edges. More often than the 3b algorithm, the retrieval using 3a tends to misclassify the thin edges of some low and midlevel clouds as cirrus and opaque ice.

The algorithm also requires a cloud mask as only satellite pixels which are fully covered by cloud should be processed. Pavolonis et al. [2005] have shown that if any clear pixels are passed to the cloud typing code, they would mostly be identified as warm liquid water or supercooled-mixed-phase cloud depending on the brightness temperature at 11 μm over most surface types and as opaque ice cloud over cold snow/ice covered surfaces.

Finally, the surface type of each single satellite pixel is required because different threshold values are applied depending on the underlying surface, particularly for water, desert and snow/ice.

[3] AVHRR sensors mounted on NOAA-7, 9, 11, 12 and 14 have only five channels (3a is missing). NOAA-15 through NOAA-19 as well as MetOp-A and MetOp-B have six channels, but only 5 channels are transmitted simultaneously, such that there is a potential switch in availability between 3a and 3b for certain time periods and sensors (generally 3a during the day and 3b during the night).

2.3 Cloud property retrieval algorithm

Although the algorithm described here is applicable to measurements in a wide range of visible to thermal infrared atmospheric window channels, within the Cloud_cci project it is being applied to the so-called *heritage channels* first used on the AVHRR series of instruments. These are six channels centred around 0.67, 0.87, 1.6, 3.7, 11, and 12 μm (although there can be considerable differences in the widths and central wavelengths of filter band-passes in different instruments). These channels are sensitive in different ways to the macro and microphysical properties of cloud. For example, the infrared channels compliment the visible channels in the case of optically thin clouds. However, the observations are not sensitive to every aspect of the three-dimensional distribution of all relevant cloud properties and no single channel is uniquely sensitive to a specific cloud property.

We approach the problem of extracting useful information on cloud as an inverse problem. A forward model (FM) is defined which applies a radiative transfer model (RTM) to simulate satellite radiances based on a parameterized cloud / atmosphere / surface model (CM) and the prescribed observing conditions. An inverse or retrieval model (RM) is then used to obtain the cloud parameters which give the best fit between the model predicted and observed radiances, taking into account measurement uncertainties and relevant prior knowledge. This inverse problem is solved using the optimal estimation method [Rodgers, 2000] (OEM).

The basic principle of the OEM is to maximise the probability of the retrieved state, conditional on the value of the measurements and any *a priori* knowledge. Formally, it maximises the conditional probability $P = P(\vec{x}|\vec{y},\ \vec{x_{\rm a}})$ with respect to the values of the measurement vector $\vec{y}$, state vector $\vec{x}$, and *a priori* estimate of the state $\vec{x}_{\rm a}$ (i.e. the most likely state prior to considering the measurements). It is assumed that errors in the measurements, forward model and *a priori* parameters are normally distributed with zero mean and covariances given by $\mathbf{S}_y$ and $\mathbf{S}_{\rm a}$, respectively. The solution state is found by minimising the cost function J:

$$J(\vec{x}) = [\vec{y}(\vec{x}) - \vec{y_{\rm m}}]\,\mathbf{S_y}^{-1}\,[\vec{y}(\vec{x}) - \vec{y_{\rm m}}]^T + (\vec{x} - \vec{x_{\rm a}})\,\mathbf{S_a}^{-1}\,(\vec{x} - \vec{x_{\rm a}})^T\,. \tag{1}$$

Starting from some initial guess of the state and linearising the forward model, the gradient of the cost function is estimated. Using that, a state is selected which is predicted to have lower cost. The Levenberg-Marquart [Marquardt, 1963, Levenberg, 1944] scheme is used to perform the minimisation. The procedure is iterated until the change in cost between iterations is less than $0.05m$, where m is the length of $\vec{y}$, (called convergence) or the retrieval is abandoned after 40 iterations.

If the *a priori* and measurement uncertainties are well represented by their respective covariances, the value of the cost function at solution is expected to be sampled from a χ^2 distribution with degrees of freedom (approximately) equal to the total number of elements in the measurement and state vectors. Hence, J at convergence provides a measure of the likelihood of the solution-state being consistent with observations and prior knowledge.

For retrievals which satisfactorily converge, i.e. converge to a minimum cost which is consistent with measurement and prior uncertainties, the uncertainty on the estimated state parameters is described by the solution covariance

$$\mathbf{S}_{\rm x} = (\mathbf{K}^T\mathbf{S}_{\rm y}^{-1}\mathbf{K} + \mathbf{S}_{\rm a}^{-1})^{-1}, \tag{2}$$

where $\mathbf{K}$ contains the derivatives of the forward model with respect to each solution state parameter:

$$K_{i,j} = \frac{\partial y_i}{\partial x_j}. \tag{3}$$

2.3.1 Cloud / Atmosphere / Surface Model

The retrieval forward model can be considered to consist of three components: a scattering cloud layer is located within a clear-sky atmosphere over a surface of known reflectance/emissivity. The clear-sky atmosphere

is defined by temperature and humidity profiles taken from ECMWF ERA Interim analyses [Dee et al., 2008]. As only window channels are being used in the retrieval, the influence of variations in trace gas concentrations, as well as the uncertainties in ECMWF water vapour profiles, are well within the measurement noise.

The surface is characterised by a bidirectional reflectance distribution function (BRDF) which is computed differently for ocean and land surface. The BRDF over ocean is computed using the methodology outlined by [Sayer et al., 2010] which includes 3 components:

$$\rho(\theta_0, \theta_v, \phi, \lambda, u, v) = \rho_{\text{sg}}(\theta_0, \theta_v, \phi, \lambda, u, v) + \rho_{\text{wc}}(\lambda, u, v) + \rho_{\text{ul}}(\theta_0, \theta_v, \lambda, C), \tag{4}$$

where ρ_{sg} is the sun-glint off wave facets [Cox and Munk, 1954a], ρ_{wc} is the reflectance from surface foam, so-called "whitecaps" [Koepke et al., 1984], and ρ_{ul} is the scattering from the within the water, so-called "underlight" [Morel et al., 1977]. In addition, physical parameters include the horizontal wind vector u and v (m/s) and the ocean pigment concentration C (mg/m^3).

The BRDF over land is a weighted sum of an isotropic kernel (unity) and two BRDF kernels [Wanner et al., 1997]

$$\rho(\theta_0, \theta_v, \phi, \lambda) = f_{\text{iso}}(\lambda) + f_{\text{vol}}(\lambda) K_{\text{vol}}(\theta_0, \theta_v, \phi) + f_{\text{geo}}(\lambda) K_{\text{geo}}(\theta_0, \theta_v, \phi), \tag{5}$$

where $K_{\text{vol}}(\theta_0, \theta_v, \phi)$ is known as the the Ross-thick kernel which parameterises *volumetric* scattering of leaves in dense vegetation and $K_{\text{geo}}(\theta_0, \theta_v, \phi)$ is the Li-sparse kernel which parameterises *geometric* shadowing in sparsely wooded vegetation. The weights $f(\lambda)$ are provided by the 0.05° MODIS MCD43C1 BRDF auxiliary input discussed in section 3.

For the infrared channels the surface is assumed to have an emissivity of unity over the ocean, while the CIMSS global land emissivity database is used [Seemann et al., 2007]. The temperature of the surface is a retrieved parameter (see section 2.3.8).

Each measurement pixel is considered to be either fully cloudy or clear. The algorithm does provide the capability of retrieving the cloud-filled fraction of a pixel, but it has been found that the heritage channels do not provide sufficient information to distinguish thin but complete cloud cover from thick but partial cover. Cloud is assumed to be a single, plane-parallel layer of either liquid or ice particles. The layer is assumed to be (geometrically) infinitely thin and is placed within the clear-sky atmosphere model. The cloud layer is parametrised in terms of the following retrieved quantities:

- The cloud phase, i.e. ice or liquid.
- The effective radius r_{eff} of the cloud particle size distribution.
- The total (vertically integrated) optical depth τ of the cloud at a fixed wavelength of 0.55 μm.
- The cloud top pressure p_{c}.

Size distributions for ice and liquid cloud are defined as a function of only r_{eff}, which defines the shape of the modelled size distribution, and τ, implicitly defining the total number of particles. For ice clouds, single-scattering properties (extinction coefficient, single-scattering albedo and phase function) are taken from Baran et al. [2004]. These are based on a mixture of ray tracing and T-Matrix methods. Size distributions are those of warm Uncinus cirrus cloud [Takano et al., 1989] which have been scaled to give a range of effective radii. Single-scattering properties of liquid cloud are derived by Mie theory assuming a modified gamma size distribution of particle radius r such that

$$n(r) = 2.373\, r^6 \exp\left(\frac{-6r}{r_m}\right), \tag{6}$$

where r_m is the mode radius of the distribution. The radiatively significant effective radius r_{eff} is given by

$$r_{\text{eff}} = \frac{\int_0^\infty r \pi r^3 n(r) dr}{\int_0^\infty \pi r^2 n(r) dr}. \tag{7}$$

This approach reduces the complexity of cloud to a simple model with parameters which can be distinguished using the heritage channels. The visible channel radiances are predominantly controlled by the cloud optical depth. Near-IR channels are also sensitive to particle size and phase due to the dependence on size of the single-scattering albedo in that spectral range and the associated differences between ice and liquid phase particles. Thermal channels predominantly provide information on cloud top pressure (via the dependence of the cloud thermal emission on the atmospheric temperature profile). It should be appreciated that all channels are sensitive, to a greater or lesser extent, to all parameters (dependant on the scene).

This simple model cannot represent all aspects of cloud three-dimensional structure. In the ideal case, the retrieved parameters should correspond to vertical (over the profile) and horizontal (over the scene) averages of the "true" cloudy properties. However, there are classes of clouds, particularly those with strong vertical variations in particle size and phase, for which this model cannot predict radiances consistent with observations in all channels. Such conditions can be identified by checking that the retrieval converges with satisfactory cost.

2.3.2 Reflectance and transmission operators

The next step in the forward model is the prediction of transmission and reflectance operators for an atmosphere *without* molecular absorption. This calculation is based on solar and viewing geometry, the molecular scattering optical thickness τ_{ms} and single-scattering phase function $P_{\mathrm{ms}}(\lambda, \Theta)$, the optical thickness $\tau_{\mathrm{a}}(\lambda)$, the single-scattering albedo $\omega_{\mathrm{a}}(\lambda)$ and the single-scattering phase function $P_{\mathrm{a}}(\lambda, \Theta)$. For performance reasons this calculation is look-up table (LUT) based from which the values for an arbitrary set of geometric and optical parameters may be interpolated. The vertices of the LUTs are computed with the DIscrete Ordinates Radiative Transfer (DISORT) software package [Stamnes et al., 1988]. It is important to note that this step, although slow, is performed off-line and the resulting look-up tables (LUTs) are static.

DISORT is a thoroughly documented and widely used general purpose algorithm for the calculation of time-independent radiative transfer. The DISORT algorithm solves the equation for the transfer of monochromatic light at wavelength λ in a medium with absorption and multiple scattering, including solar and thermal sources. The radiative transfer equation is written as

$$\mu \frac{dL_\lambda(\tau_\lambda, \mu, \phi)}{d\tau} = L_\lambda(\tau_\lambda, \mu, \phi) - J_\lambda(\tau_\lambda, \mu, \phi), \tag{8}$$

where $L_\lambda(\tau_\lambda, \mu, \phi)$ is the intensity along direction μ, ϕ (where μ is the cosine of the zenith angle and ϕ is the azimuth angle) at optical depth τ_λ measured perpendicular to the surface of the medium. $J_\lambda(\tau_\lambda, \mu, \phi)$ is the source function, which can include solar and thermal sources.

It should be noted that DISORT still makes some important approximations, which can limit its accuracy in certain circumstances. The most important of these are:

- It assumes a plane parallel atmosphere, which makes it inapplicable at viewing or zenith angles above approximately $75°$, where the curvature of the Earth has a significant influence on radiative transfer.
- It is a one-dimensional model, so cannot reproduce the effects of horizontal gradients in the scattering medium. This is important where strong gradients exist, such as near cloud edges.
- It does not model polarisation effects and hence cannot be used to model measurements made by instruments which are sensitive to polarisation and does not take into account the polarisation introduced into the diffuse component of radiance by molecular scattering.

DISORT is provided with solar and instrument geometry, the molecular scattering and cloud radiative properties at the vertexes. The transmission and reflectance of the atmosphere is computed for both direct beam and diffuse radiation sources separately. The calculations are performed quasi-monochromatically, i.e. a single radiative transfer calculation is performed for each channel. It is the input optical properties that are

convolved to the instrument's response function for a particular channel. These calculations produce six LUTs for each channel:

- $R_{\mathrm{bb}}(\theta_0, \theta_{\mathrm{v}}, \phi)$: the bidirectional reflectance of the cloud.
- $T^{\downarrow}_{\mathrm{bb}}(\theta_0)$: the downward direct transmission of the cloud of the direct solar beam.
- $T^{\uparrow}_{\mathrm{bb}}(\theta_{\mathrm{v}})$: the upward direct transmission of the cloud into the viewing direction.
- $T^{\downarrow}_{\mathrm{bd}}(\theta_0)$: the downward diffuse transmission of the cloud, as illuminated by the direct solar beam.
- $T^{\uparrow}_{\mathrm{db}}(\theta_{\mathrm{v}})$: the upward diffuse transmission of the cloud, as viewed from a specific direction.
- R_{dd}: the bi-hemispherical reflectance of the cloud.

Here, a $\downarrow$ denotes transmission from the top to the bottom of the atmosphere, while $\uparrow$ indicates the reverse. Dependence on the solar zenith, viewing zenith and relative azimuth angles are denoted by θ_0, θ_{v} and ϕ respectively. The pairs of b and d subscripts denote the type of radiation each term operates on and produces; for example $T^{\downarrow}_{\mathrm{bd}}(\lambda, \theta_0)$ operates on the direct beam (b) of solar radiation, and produces the diffuse radiation (d) that results at the bottom of the atmosphere. Each of these tables contains tabulated transmission or reflectance (depending on the table) values for each of the ten equally spaced solar and/or sensor zenith angles, eleven equally spaced relative azimuth angles ($R_{\mathrm{bb}}(\lambda, \theta_0, \theta_{\mathrm{v}}, \phi)$ only), eighteen 0.55 μm optical depths and twenty three effective radii.

2.3.3 Surface reflectance operators

The CC4CL forward model works on the assumption that the surface BRDF can be parameterized by four reflectance terms:

1. The bidirectional reflectance, $\rho_{\mathrm{bb}}(\lambda, \theta_0, \theta_{\mathrm{v}}, \phi)$. This is the reflectance of the surface to direct beam illumination at θ_0, as viewed from a specific direction θ_{v}. It is the reflectance that would be observed by a satellite instrument in the absence of an atmosphere.

2. The directional-hemispheric reflectance $\rho_{\mathrm{bd}}(\lambda, \theta_0)$. This is the fraction of incoming direct beam illumination at θ_0 that is reflected across all viewing angles. This is also referred to as the *black-sky albedo*.

3. The hemispheric-directional reflectance $\rho_{\mathrm{db}}(\lambda, \theta_{\mathrm{v}})$. This is the reflectance of the surface to purely diffuse illumination, as viewed from a specific direction θ_{v}.

4. The bi-hemispheric reflectance $\rho_{\mathrm{dd}}(\lambda)$. This is the reflectance of the surface to purely diffuse illumination, across all viewing directions. This is also referred to as the *white-sky albedo*.

The first term $\rho_{\mathrm{bb}}(\theta_0, \theta_{\mathrm{v}}, \phi)$ is computed directly from the BRDF. The three other terms are derived from the BRDF integrated over solar and/or viewing geometry written as

$$\begin{aligned}\rho_{\mathrm{bd}}(\lambda, \theta_0) &= \frac{\int_0^{2\pi}\int_0^{\pi/2} \rho_{\mathrm{bb}}(\lambda, \theta_0, \theta_{\mathrm{v}}, \phi)\cos\theta_{\mathrm{v}}\sin\theta_{\mathrm{v}}\mathrm{d}\theta_{\mathrm{v}}\mathrm{d}\phi}{\int_0^{2\pi}\int_0^{\pi/2}\cos\theta_{\mathrm{v}}\sin\theta_{\mathrm{v}}\mathrm{d}\theta_{\mathrm{v}}\mathrm{d}\phi} \\ &= \frac{1}{\pi}\int_0^{2\pi}\int_0^{\pi/2} \rho_{\mathrm{bb}}(\lambda, \theta_0, \theta_{\mathrm{v}}, \phi)\cos\theta_{\mathrm{v}}\sin\theta_{\mathrm{v}}\mathrm{d}\theta_{\mathrm{v}}\mathrm{d}\phi,\end{aligned} \tag{9}$$

$$\begin{aligned}\rho_{\mathrm{db}}(\lambda,\theta_{\mathrm{v}}) &= \frac{\int_0^{2\pi}\int_0^{\pi/2}\rho_{\mathrm{bb}}(\lambda,\theta_0,\theta_{\mathrm{v}},\phi)\cos\theta_{\mathrm{v}}\sin\theta_{\mathrm{v}}\mathrm{d}\theta_0\mathrm{d}\phi}{\int_0^{2\pi}\int_0^{\pi/2}\cos\theta_{\mathrm{v}}\sin\theta_{\mathrm{v}}\mathrm{d}\theta_0\mathrm{d}\phi} \\ &= \frac{1}{\pi}\int_0^{2\pi}\int_0^{\pi/2}\rho_{\mathrm{bb}}(\lambda,\theta_0,\theta_{\mathrm{v}},\phi)\cos\theta_{\mathrm{v}}\sin\theta_{\mathrm{v}}\mathrm{d}\theta_0\mathrm{d}\phi,\end{aligned} \tag{10}$$

$$\begin{aligned}\rho_{\mathrm{dd}}(\lambda) &= \frac{\int_0^{\pi/2}\rho_{\mathrm{bd}}(\lambda,\theta_0)\cos\theta_0\sin\theta_0\mathrm{d}\theta_0}{\int_0^{\pi/2}\cos\theta_0\sin\theta_0\mathrm{d}\theta_0} \\ &= 2\int_0^{\pi/2}\rho_{\mathrm{bd}}(\lambda,\theta_0)\cos\theta_0\sin\theta_0\mathrm{d}\theta_0.\end{aligned} \tag{11}$$

2.3.4 Visible and near-IR RTM

Each short wave channel measures the radiance in the instrument's field-of-view, defined by the solid angle Δ_{FOV}. Each channel also has a relative spectral response $\varrho(\lambda)$ within a wavelength interval $[\lambda_1,\lambda_2]$ and has zero response outside this band. Under these conditions the radiance measured by the instrument is

$$L^r_{\bar{\lambda}}(\omega_r) = \frac{\int_0^{\Delta_{\mathrm{FOV}}}\int_{\lambda_1}^{\lambda_2} L^r_\lambda(\lambda,\omega)\varrho(\lambda)\,d\lambda\,d\omega}{\int_0^{\Delta_{\mathrm{FOV}}}\,d\omega}, \tag{12}$$

where ω is used to represent the spherical coordinate zenith and azimuth angle pair (θ,ϕ) and the integral over solid angle has been abbreviated as

$$\int_0^{\Delta\omega} d\omega \quad = \quad \int_0^{2\pi}\int_0^{\Delta\theta}\sin\theta\,d\theta\,d\phi. \tag{13}$$

The 'Sun-normalised radiance' (or top-of-atmosphere reflectance) can then be formed by dividing the measured radiance $L^r_{\bar{\lambda}}(\omega_r)$ by $E^0_{\bar{\lambda}}$, the irradiance the satellite would measure if viewing the Sun through a perfect diffuser i.e.

$$R(\bar{\lambda},\omega_0,\omega_r) = \frac{\pi L^r_{\bar{\lambda}}(\omega_r)}{\cos\theta_0 E^0_{\bar{\lambda}}}. \tag{14}$$

The factor $\cos\theta_0$ accounts for the reduction in energy per unit area when the Suns energy strikes the atmosphere-Earth system at an angle θ_0 to the local vertical.

In the limit of a very narrow band, the measured Sun normalised radiance is a good approximation to the spectral bidirectional reflectance factor $R(\lambda,\omega_i,\omega_r)$, which is defined as the ratio of the reflected radiant flux to the reflected radiant flux from an ideal diffuse (i.e. Lambertian) surface [Schaepman-Strub et al., 2006]. The bidirectional reflectance factor is a function of the wavelength λ and the input and output directions (represented by ω_i and ω_r, respectively). For simplicity, the dependence of reflection and transmittance on λ will not be explicitly shown.

The cloudy fraction of the atmosphere in a scene is modelled with three layers: a below-cloud layer, a cloud layer and an above-cloud layer. The above and below-cloud layers consist of gaseous absorbers that attenuate radiation without scattering[4].

The gaseous absorption optical depth of the atmosphere is calculated using visible channel coefficients for RTTOV version 11.0 and the clear sky contribution for each scene is calculated with NWP information provided by 6-hourly ECMWF ERA Interim analyses. This total absorption optical depth is then partitioned

[4]Molecular scattering throughout the atmospheric column is included in the scattering calculations carried out for the cloud layer

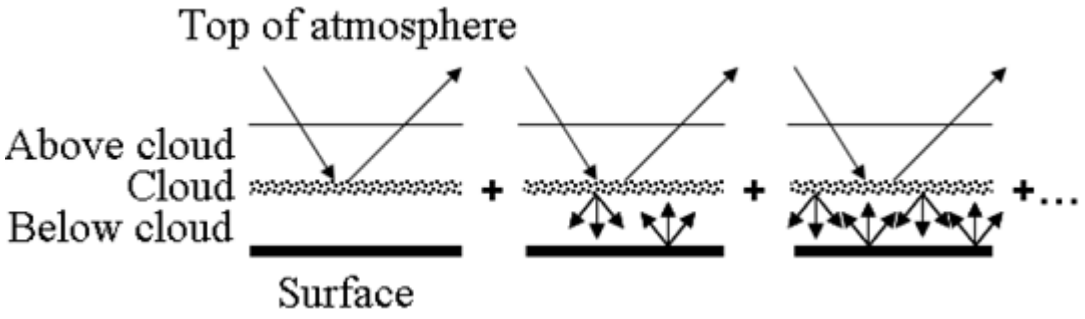

Figure 2: Schematic of the contributions to the measured radiance though multiple scattering between the atmosphere and surface.

into the above-cloud optical depth $\tau_{\rm ac}$ and the below-cloud optical depth $\tau_{\rm bc}$ based on the cloud top pressure relative to the surface pressure.

Using the reflectance and transmission operators described in section 2.3.2, the surface reflectance description in section 2.3.3, and by neglecting molecular absorption, the observed reflectance of the atmosphere/surface system can be written as (assuming dependence on wavelength λ):

$$
\begin{aligned}
R(\theta_0,\theta_{\rm v},\phi) = \; & R_{\rm bb}(\theta_0,\theta_{\rm v},\phi) && \}\text{Reflection off the atmosphere}\\
& +T^{\downarrow}_{\rm bb}(\theta_0)\rho_{\rm bb}(\theta_0,\theta_{\rm v},\phi)T^{\uparrow}_{\rm bb}(\theta_{\rm v}) &&\\
& +T^{\downarrow}_{\rm bb}(\theta_0)\rho_{\rm bd}(\theta_0)T^{\uparrow}_{\rm db}(\theta_{\rm v}) && \Big\}\text{Single reflection off the surface}\\
& +T^{\downarrow}_{\rm bd}(\theta_0)\rho_{\rm db}(\theta_{\rm v})T^{\uparrow}_{\rm bb}(\theta_{\rm v}) &&\\
& +T^{\downarrow}_{\rm bd}(\theta_0)\rho_{\rm dd}T^{\uparrow}_{\rm db}(\theta_{\rm v}) &&\\
& +T^{\downarrow}_{\rm bb}(\theta_0)\rho_{\rm bd}(\theta_0)R_{\rm dd}\rho_{\rm db}T^{\uparrow}_{\rm bb}(\theta_{\rm v}) &&\\
& +T^{\downarrow}_{\rm bb}(\theta_0)\rho_{\rm bd}(\theta_0)R_{\rm dd}\rho_{\rm dd}T^{\uparrow}_{\rm db}(\theta_{\rm v}) && \Big\}\text{Double reflection off the surface}\\
& +T^{\downarrow}_{\rm bd}(\theta_0)\rho_{\rm dd}R_{\rm dd}\rho_{\rm db}T^{\uparrow}_{\rm bb}(\theta_{\rm v}) &&\\
& +T^{\downarrow}_{\rm bd}(\theta_0)\rho_{\rm dd}R_{\rm dd}\rho_{\rm dd}T^{\uparrow}_{\rm db}(\theta_{\rm v}) &&\\
& +T^{\downarrow}_{\rm bb}(\theta_0)\rho_{\rm bd}(\theta_0)R_{\rm dd}\rho_{\rm dd}R_{\rm dd}\rho_{\rm db}T^{\uparrow}_{\rm bb}(\theta_{\rm v}) &&\\
& +T^{\downarrow}_{\rm bb}(\theta_0)\rho_{\rm bd}(\theta_0)R_{\rm dd}\rho_{\rm dd}R_{\rm dd}\rho_{\rm dd}T^{\uparrow}_{\rm db}(\theta_{\rm v}) && \Big\}\text{Triple reflection off the surface}\\
& +T^{\downarrow}_{\rm bd}(\theta_0)\rho_{\rm dd}R_{\rm dd}\rho_{\rm dd}R_{\rm dd}\rho_{\rm db}T^{\uparrow}_{\rm bb}(\theta_{\rm v}) &&\\
& +T^{\downarrow}_{\rm bd}(\theta_0)\rho_{\rm dd}R_{\rm dd}\rho_{\rm dd}R_{\rm dd}\rho_{\rm dd}T^{\uparrow}_{\rm db}(\theta_{\rm v}) &&\\
& +\ldots &&
\end{aligned}
\tag{15}
$$

Here we have four terms resulting from a single surface reflection in equation 15, which can be described as follows:

- $T^{\downarrow}_{\rm bb}(\theta_0)\rho_{\rm bb}(\theta_0,\theta_{\rm v},\phi)T^{\uparrow}_{\rm bb}(\theta_{\rm v})$ is the direct transmission of the solar beam, reflected off the surface and transmitted directly to the satellite.
- In $T^{\downarrow}_{\rm bb}(\theta_0)\rho_{\rm bd}(\theta_0)T^{\uparrow}_{\rm db}(\theta_{\rm v})$ the diffusely reflected portion of the directly transmitted solar beam is diffusely transmitted (via multiple scattering in the atmosphere) into the viewing direction of the satellite.
- $T^{\downarrow}_{\rm bd}(\theta_0)\rho_{\rm db}(\theta_{\rm v})T^{\uparrow}_{\rm bb}(\theta_{\rm v})$ gives the portion of the diffusely transmitted solar beam, which is then reflected into the viewing direction of the satellite and directly transmitted back through the atmosphere.
- $T^{\downarrow}_{\rm bd}(\theta_0)\rho_{\rm dd}T^{\uparrow}_{\rm db}(\theta_{\rm v})$ is the purely diffuse component, where solar radiation is diffusely transmitted to the surface, reflected off the surface and diffusely transmitted to the satellite.

The terms following on from these describe the rapidly diminishing series of multiple reflections between the surface and overlaying atmosphere. For these terms the assumption has been made that ground and atmosphere pair are essentially Lambertian reflectors (i.e. that only the bi-hemispherical reflectance of the atmosphere is needed). Neglecting directly transmitted solar radiation, this is equivalent to saying the sky is equally bright in all directions.

By gathering terms, equation 15 can be simplified to give

$$\begin{aligned} R = & R_{\mathrm{bb}}(\theta_0, \theta_{\mathrm{v}}, \phi) \\ & + T^{\downarrow}_{\mathrm{bb}}(\theta_0)\rho_{\mathrm{bb}}(\theta_0, \theta_{\mathrm{v}}, \phi)T^{\uparrow}_{\mathrm{bb}}(\theta_{\mathrm{v}}) + T^{\downarrow}_{\mathrm{bd}}(\theta_0)\rho_{\mathrm{db}}(\theta_{\mathrm{v}})T^{\uparrow}_{\mathrm{bb}}(\theta_{\mathrm{v}}) \\ & + \left(T^{\downarrow}_{\mathrm{bb}}\theta_0)\rho_{\mathrm{bd}}(\theta_0) + T^{\downarrow}_{\mathrm{bd}}(\theta_0)\rho_{\mathrm{dd}}\right) T^{\uparrow}_{\mathrm{db}}(\theta_{\mathrm{v}}) \left(1 + \rho_{\mathrm{dd}}R_{\mathrm{dd}} + \rho^2_{\mathrm{dd}}R^2_{\mathrm{dd}} + ...\right) \\ & + \left(T^{\downarrow}_{\mathrm{bb}}(\theta_0)\rho_{\mathrm{bd}}(\theta_0) + T^{\downarrow}_{\mathrm{bd}}(\theta_0)\rho_{\mathrm{dd}}\right) R_{\mathrm{dd}}\rho_{\mathrm{db}}(\theta_{\mathrm{v}})T^{\uparrow}_{\mathrm{bb}}(\theta_{\mathrm{v}}) \left(1 + \rho_{\mathrm{dd}}R_{\mathrm{dd}} + \rho^2_{\mathrm{dd}}R^2_{\mathrm{dd}} + ...\right). \end{aligned} \tag{16}$$

This can then be further simplified, using the appropriate series limit, to give

$$\begin{aligned} R = & R_{\mathrm{bb}}(\theta_0, \theta_{\mathrm{v}}, \phi) \\ & + T^{\downarrow}_{\mathrm{bb}}(\theta_0)\rho_{bb}(\theta_0, \theta_{\mathrm{v}}, \phi)T^{\uparrow}_{\mathrm{bb}}(\theta_{\mathrm{v}}) + T^{\downarrow}_{\mathrm{bd}}(\theta_0)\rho_{\mathrm{db}}(\theta_{\mathrm{v}})T^{\uparrow}_{\mathrm{bb}}(\theta_{\mathrm{v}}) \\ & + \frac{\left(T^{\downarrow}_{\mathrm{bb}}(\theta_0)\rho_{\mathrm{bd}}(\theta_0) + T^{\downarrow}_{\mathrm{bd}}(\theta_0)\rho_{\mathrm{dd}}\right)\left(T^{\uparrow}_{\mathrm{db}}(\theta_{\mathrm{v}}) + R_{\mathrm{dd}}\rho_{\mathrm{db}}(\theta_{\mathrm{v}})T^{\uparrow}_{\mathrm{bb}}(\theta_{\mathrm{v}})\right)}{1 - \rho_{\mathrm{dd}}R_{\mathrm{dd}}}. \end{aligned} \tag{17}$$

Finally, the observed TOA reflectance including molecular absorption is obtained by scaling the terms in equation 17 by the appropriate clear-sky transmission terms

$$\begin{aligned} R_{\mathrm{TOA}} = & \mathcal{T}_{\mathrm{ac}}(\theta_0)\mathcal{T}_{\mathrm{ac}}(\theta_{\mathrm{v}}) \left[R_{\mathrm{bb}}(\theta_0, \theta_{\mathrm{v}}, \phi)\right. \\ & + \mathcal{T}_{\mathrm{bc}}(\theta_0)T^{\downarrow}_{\mathrm{bb}}(\theta_0)\rho_{bb}(\theta_0, \theta_{\mathrm{v}}, \phi)T^{\uparrow}_{\mathrm{bb}}(\theta_{\mathrm{v}})\mathcal{T}_{\mathrm{bc}}(\theta_{\mathrm{v}}) + \mathcal{T}_{\mathrm{bc}}(0)T^{\downarrow}_{\mathrm{bd}}(\theta_0)\rho_{\mathrm{db}}(\theta_{\mathrm{v}})T^{\uparrow}_{\mathrm{bb}}(\theta_{\mathrm{v}})\mathcal{T}_{\mathrm{bc}}(\theta_{\mathrm{v}}) \\ & \left. + \frac{\left(\mathcal{T}_{\mathrm{bc}}(\theta_0)T^{\downarrow}_{\mathrm{bb}}(\theta_0)\rho_{\mathrm{bd}}(\theta_0) + \mathcal{T}_{\mathrm{bc}}(0)T^{\downarrow}_{\mathrm{bd}}(\theta_0)\rho_{\mathrm{dd}}\right)\left(\mathcal{T}_{\mathrm{bc}}(0)T^{\uparrow}_{\mathrm{db}}(\theta_{\mathrm{v}}) + R_{\mathrm{dd}}\mathcal{T}^2_{\mathrm{bc}}(0)\rho_{\mathrm{db}}(\theta_{\mathrm{v}})T^{\uparrow}_{\mathrm{bb}}(\theta_{\mathrm{v}})\mathcal{T}_{\mathrm{bc}}(\theta_{\mathrm{v}})\right)}{1 - \rho_{\mathrm{dd}}R_{\mathrm{dd}}\mathcal{T}^2_{\mathrm{bc}}(0)}\right], \end{aligned} \tag{18}$$

where $\mathcal{T}_{\mathrm{ac}}(\theta) = e^{-\tau_{\mathrm{ac}}/\cos\theta}$, $\mathcal{T}_{\mathrm{bc}}(\theta) = e^{-\tau_{\mathrm{bc}}/\cos\theta}$, τ_{ac} and τ_{bc} are the above cloud and below cloud optical thicknesses, respectively, and it is assumed that the mean angle of diffuse transmission is 66°.

2.3.5 Thermal-IR RTM

The thermal RTM makes extensive use of the RTTOV model [Saunders et al., 1999]. RTTOV directly provides the modelled radiance from the clear-sky fraction of the scene.

The observed cloudy brightness temperature is given by

$$L^{\uparrow}(\theta_v) = L^{\uparrow}_{ac}(\theta_{\mathrm{v}}) + \left(L^{\downarrow}_{\mathrm{ac}}R^{\uparrow}_{\mathrm{db}}(\theta_{\mathrm{v}}) + B(T_{\mathrm{c}})\varepsilon_{\mathrm{c}} + L^{\uparrow}_{bc}T^{\uparrow}_{\mathrm{db}}(\theta_{\mathrm{v}})\right) e^{-(\tau_{\mathrm{ac}}/\cos\theta_{\mathrm{v}})}, \tag{19}$$

where $L^{\uparrow}_{ac}(\theta_{\mathrm{v}})$ is the upward radiance into the viewing direction from the atmosphere above the cloud, $L^{\downarrow}_{ac}$ is the downward radiance from the atmosphere above the cloud, $L^{\uparrow}_{bc}$ is the upward radiance from the atmosphere below the cloud, $B(T_{\mathrm{c}})$ is the Planck function as a function of the cloud top temperature T_{c}, ε_{c} is the cloud emissivity obtained from an LUT computed in a similar way as those for the operators R and T and $e^{-(\tau_{\mathrm{ac}}/\cos\theta_{\mathrm{v}})}$ is the transmission from TOA to the cloud top. The transmission term $e^{-(\tau_{\mathrm{ac}}/\cos\theta_{\mathrm{v}})}$ is obtained from transmission profiles computed with RTTOV while the clear-sky radiance terms L are obtained from thermal emission profiles computed with RTTOV.

2.3.6 Derivatives of the forward model

The gradient of the forward model $\partial y_i/\partial x(j$, where y_i is a radiance measurement in a single channel and x_j is one of the retrieved parameters, is required for the following purposes:

1. The gradient with respect to parameters which are to be derived from the measurements (state parameters) is a vital quantity for the inversion of the non-linear reflectance model by the Levenberg-Marquardt algorithm.

2. The gradient with respect to parameters which might be considered known and not part of the inversion procedure (model parameters such as surface reflectance spectral shape) is used to judge the sensitivity to these parameters and thus to estimate their contribution to the retrieval uncertainty.

Derivatives of the forward model may be obtained through straightforward linearisation of the forward model equations already given and as a result will not be listed here.

2.3.7 Single layer Measurement vector and covariance

The retrieval scheme described here uses nadir-view observations in the 0.67, 0.87, 1.6, 3.7, 11 and 12 μm channels. In practice only one of the 1.6 or 3.7 μm channels is included in a given retrieval because it has been found to be difficult to consistently represent both the 1.6 and 3.7 μm channels with the simple CM used [Baran et al., 2004]. Similarly, forward view radiances are not included as the three-dimensional structure of cloud will often cause differences between the views which cannot be accommodated by the simple model. The error covariance used in the retrieval is the sum of three terms:

$$\mathbf{S}_y = \mathbf{S}_{\text{noise}} + \mathbf{S}_{\text{pixel}} + \mathbf{S}_{\text{fm}}. \tag{20}$$

- $\mathbf{S}_{\text{noise}}$ represents random instrument noise on the observations. The matrix is assumed diagonal with values on the diagonal equal to the square of the assumed measurement noise, which are set for each instrument based on pre-launch characterisation.

- $\mathbf{S}_{\text{pixel}}$ represents errors related to inadequacies of the plane-parallel cloud model and imperfect co-registration of the channels. It is assumed diagonal and equal to the square of 2 % of the measured radiance for visible and near-IR channels[5]. and 0.08 K for the thermal channels. These are combined for the mixed 3.7 μm channel[6]. See Watts et al. [1998] for the derivation of this term.

- $\mathbf{S}_{\text{fm}}$ is zero for rows and columns corresponding to thermal channels. For the visible and near-IR channels, the matrix represents uncertainties in the MODIS surface albedo. Diagonal elements are set to (the square of) 20 % of the albedo for the corresponding channel. Off-diagonals are set to give a correlation between the visible/near-IR channels of 0.2.

2.3.8 State vector and a priori constraint

The state-vector used in the retrieval prescribes:

- Log_{10} optical depth;

- Cloud effective radius;

- Cloud top pressure;

[5] For ATSR-2 channel 4, the visible uncertainty is 1.5 %.

[6] For mixed channels, the radiance is converted into an equivalent brightness temperature.

- Surface temperature.

A priori and first guess values depend on the assumed phase (phase determination is addressed in section 2.2). For liquid cloud, *a priori* values are 6.3, 12 μm and 900 hPa for optical depth, effective radius and cloud top pressure, respectively; for ice the equivalent values are are 6.3, 30 μm and 400 hPa. The surface temperature *a priori* value is taken from ECMWF reanalysis fields for the skin temperature.

In the absence of useful information, the *a priori* uncertainty for the state parameters is set to 10^8 for optical depth, effective radius, and cloud top pressure. This implies that these parameters are effectively unconstrained by their *a priori* value. For surface temperature, the *a priori* uncertainty is set to 2 K over sea and 5 K over land. The *a priori* covariance is assumed to be diagonal.

The initial (first guess) values for state-vector parameters are set equal to the *a priori* values, except cloud top pressure which is set by:

- Find the channel with wavenumber less than 2500 cm^{-1} that is nearest to 909 cm^{-1}. If there is no such channel, do not attempt a retrieval.
- Convert the brightness temperature in that channel to a radiance. If the pixel is flagged as clear, subtract the TOA clear-sky radiance (as given by the LUT for that channel).
- If that radiance is less than zero, use the first guess specified above. Otherwise, convert the radiance into a brightness temperature and interpolate it onto the ECMWF temperature profile to find the first guess cloud top pressure.

2.3.9 Cloud Albedo

Given the reflection function is parameterised as a function of waveband, input and output geometry and cloud properties (optical depth, effective radius and phase), it is possible to output three reflection terms:

- The cloud reflection factor for the Sun-cloud-satellite geometry $R(\mu_0, \phi_0; \mu, \phi)$;
- The directional-hemispherical reflectance for unidirectional illumination (also called the black-sky albedo)

$$R(\mu_o) = \frac{1}{\pi} \int_0^{2\pi} \int_0^1 R(\mu_0, \phi_0; \mu, \phi) \mu \, d\mu \, d\phi; \tag{21}$$

- The cloud bihemispherical reflectance for isotropic illumination (also called the white-sky albedo)

$$R = \frac{1}{\pi^2} \int_0^{2\pi} \int_0^1 \int_0^{2\pi} \int_0^1 R(\mu_0, \phi_0; \mu, \phi) \mu \, d\mu \, d\phi \, \mu_0 \, d\mu_0 \, d\phi_0. \tag{22}$$

Note that these terms are calculated in the absence of knowledge of the underlying surface so they refer to a cloud property alone.

The black-sky albedo is currently the reported cloud albedo in the CCI product.

2.3.10 Corrected CTT, CTP and CTH

The temperature of the geometric top of the cloud, which we have named as the *corrected* cloud top temperature $T_{\mathrm{c,cor}}$, in contrast to the retrieved radiative cloud top temperature T_{c} (CTT), may be written as

$$T_{\mathrm{c,cor}} = \mathrm{BT_c}(\lambda) + \Gamma \Delta Z, \tag{23}$$

where $\mathrm{BT_c}(\lambda)$ is the brightness temperature (K) at wavelength λ observed from the *top of the cloud*, Γ is the atmospheric lapse rate (-K/km) and ΔZ (km) is the geometric depth into the cloud of T_{c}.

If we assume that the cloud is vertically homogeneous the cloud optical depth $\Delta\tau_{\rm c}(\lambda)$ at a geometric depth ΔZ (km) into the cloud is given by

$$\Delta\tau_{\rm c}(\lambda) = \sigma_{\rm c}(\lambda) N_{\rm c} \Delta Z, \tag{24}$$

where $\sigma_{\rm c}(\lambda)$ is the size distribution averaged cloud particle cross section and N is the cloud particle number concentration ($1/\mathrm{km}^3$). If we assume that the peak sensitivity to $T_{\rm c}$ comes from one optical depth into the cloud ($\Delta\tau_{\rm c} = 1$) then ΔZ may be written as

$$\Delta Z = \frac{1}{\sigma_{\rm c}(\lambda) N_{\rm c}}. \tag{25}$$

From equation 23, two equations may be formed, for measurements at 11 and 12 , respectively:

$$T_{\rm c,cor} = \mathrm{BT}_{\rm c}(11) + \frac{\Gamma}{\sigma_{\rm c}(11) N_{\rm c}}, \tag{26}$$

$$T_{\rm c,cor} = \mathrm{BT}_{\rm c}(12) + \frac{\Gamma}{\sigma_{\rm c}(12) N_{\rm c}}, \tag{27}$$

where there are two unknowns, $T_{\rm c,cor}$ and $\Gamma/N_{\rm c}$. By solving for $\Gamma/N_{\rm c}$ with each equation and equating the results as

$$\sigma_{\rm c}(11)\left[T_{\rm c,cor} - \mathrm{BT}_{\rm c}(11)\right] = \sigma_{\rm c}(12)\left[T_{\rm c,cor} - \mathrm{BT}_{\rm c}(12)\right], \tag{28}$$

$T_{\rm c,cor}$ may be solved for, given by

$$T_{\rm c,cor} = \frac{\sigma_{\rm c}(11)\mathrm{BT}_{\rm c}(11) - \sigma_{\rm c}(12)\mathrm{BT}_{\rm c}(11)}{\sigma_{\rm c}(11) - \sigma_{\rm c}(12)}. \tag{29}$$

The brightness temperatures as observed from the top of the cloud, $\mathrm{BT}_{\rm c}(\lambda)$ may be obtained from the corresponding brightness temperatures observed at TOA $\mathrm{BT}_{\rm TOA}(\lambda)$ with

$$\mathrm{BT}_{\rm c}(\lambda) = \mathrm{BT}_{\rm TOA}(\lambda)/\mathcal{T}_{\rm ab}(\lambda), \tag{30}$$

where $\mathcal{T}_{\rm ab}(\lambda)$ is the above cloud clear-sky atmospheric transmittance, i.e. the transmittance from TOA to the top of the cloud, along the satellite viewing slant path. Cloud particle cross section $\sigma_{\rm c}(\lambda)$ is obtained from pre-computed LUTs as a function of wavelength and the retrieved cloud optical thickness (COT) and cloud effective radius (CER).

The corresponding corrected cloud top pressure $P_{\rm c,cor}$ and corrected cloud top height $H_{\rm c,cor}$ may be obtained from the input pressure and temperature profiles simply by comparing $T_{\rm c,cor}$ with the input temperature profile and interpolating appropriately.

The estimated uncertainties of $T_{\rm c,cor}$, $P_{\rm c,cor}$ and $H_{\rm c,cor}$ are obtained through straight forward error propagation, the details of which will not be discussed here.

2.3.11 Boundary layer inversion

A boundary layer temperature inversion can often permit two valid solutions for the cloud top pressure within the OEM retrieval, depending on whether one searches the temperature profile from top to bottom or vice versa. Thus, the retrieved height may either be too high or too low. The following solution is derived from the Meteosat Third Generation Level 2 Processing Specification Document [EUMETSAT, 2014] but is repeated here as that document is not easily accessible:

- Search from the bottom of the forecast temperature profile for a typical anticyclonic temperature inversion. Numbering the levels of the forecast model from 1 at the surface to N at TOA, an inversion is identified by the smallest $1 < i < N$ where $T^i_{\rm fcst} < T^{i+1}_{\rm fcst} - 1\,\mathrm{K}$ and $T^i_{\rm fcst} < T^{i-1}_{\rm fcst}$ with $P^i_{\rm fcst} > 600\,\mathrm{hPa}$ (where $T^i_{\rm fcst}$ and $P^i_{\rm fcst}$ are the temperature and pressure at forecast level i, respectively). Eventually, this scheme should be extended to account for the humidity profile.

- The top of the inversion is identified as the smallest $j \geq i+2$ at which $T^{j}_{\text{fcst}} < T^{j-1}_{\text{fcst}}$.
- If no inversion is found, the forecast temperature profile is retained. Otherwise, modify the temperature profile within the inversion to facilitate a more sensible cloud top pressure retrieval. This extrapolates the boundary layer below the inversion such that:

$$T^{k} = \begin{cases} T^{i}_{\text{fcst}} + \Gamma_{\text{BL}} \left(P^{k}_{\text{fcst}} - P^{i}_{\text{fcst}} \right) & i < k \leq j+2 \\ T^{k}_{\text{fcst}} & \text{otherwise,} \end{cases} \tag{31}$$

  where the boundary layer lapse rate Γ_{BL} is approximated from the levels beneath the inversion,

$$\Gamma_{\text{BL}} = \frac{\mathrm{d}T}{\mathrm{d}P} \simeq \frac{T^{i-1}_{\text{fcst}} - T^{i-2}_{\text{fcst}}}{P^{i-1}_{\text{fcst}} - P^{i-2}_{\text{fcst}}}. \tag{32}$$

- The $+2$ in eqn. 31 and the second step account for uncertainty in the bounding of the inversion due to forecast model errors and smoothing.

2.3.12 Tropopause Identification and temperature profile modification

Occasionally deep convective clouds rise above the tropopause and there is a delay before this is expressed in the temperature profile. If not corrected, the retrieved cloud top height will be too low. This is accounted for, equivalent to Section 2.3.11, by extrapolating from the temperature profile just below the tropopause:

- The tropopause is identified by the largest $i < N$ where $T^{i} > T^{i+1}$, $T^{i-2} - T^{i-1} > 2\,\text{K}$ and $P^{i+1}_{\text{fcst}} > 80\,\text{hPa}$.
- The temperature profile is then modified such that:

$$T^{k}_{\text{modified}} = \begin{cases} T^{i} + \Gamma_{\text{troposphere}} \left(P^{k}_{\text{fcst}} - P^{i}_{\text{fcst}} \right) & i < k \leq N \\ T^{k} & \text{otherwise,} \end{cases} \tag{33}$$

  where the tropospheric lapse rate $\Gamma_{\text{troposphere}}$ is approximated from the levels beneath the tropopause,

$$\Gamma_{\text{troposphere}} = \frac{T^{i-2}_{\text{fcst}} - T^{i}_{\text{fcst}}}{P^{i-2}_{\text{fcst}} - P^{i}_{\text{fcst}}}. \tag{34}$$

2.3.13 ECMWF data

Clear-sky atmospheric radiances and transmittances are determined by RTTOV. This requires meteorological information as an input, which is provided by ECMWF ERA Interim reanalysis fields [Dee et al., 2008]. The required data[7] are stored in one or more files of NetCDF or GRIB format. The data presents values and profiles representative of the atmosphere and surface at each point on a reduced Gaussian grid (with resolution dependent on the data source). ORAC retrieves states averaged over each satellite pixel and, to reduce computational expense, only evaluates RTTOV on a regular 500-by-500 latitude-longitude grid, which is then linearly interpolated onto each satellite pixel. (The errors from this process have been found to be less than the uncertainties in the RTTOV calculations themselves and so are considered negligible.)

The ECMWF data must be interpolated onto the ORAC grid. As the ECMWF data is generally on a coarser grid than that used by ORAC, the grid-cell average is approximated by the ECMWF value at the cell centre. The interpolation is performed using the EMOSLIB library provided by ECMWF (found at `software.ecmwf.int/wiki/display/EMOS/Emoslib`).

[7] Currently, the fields `temperature`, `spec_hum`, `ozone`, `geopot`, `lnsp`, `sea_ice_cover`, `snow_albedo`, `sst`, `totcolwv`, `snow_depth`, `u10`, `v10`, `temp2`, `land_sea_mask` and `skin_temp` are required.

2.3.14 Night retrievals

The CC4CL cloud scheme maintains the flexibility to increase or decrease the number of channels used in the retrievals and thus increase or decrease the information content. At night, there are three usable channels — 3.7, 11 and 12 μm — and the absence of visible channels results in a reduction of the information content in the measurements with a corresponding reduction in the number of cloud parameters that can be retrieved. Currently, only cloud top pressure and surface temperature are retrieved. Optical depth and/or effective radius could be retrieved only with the application of additional constraints.

The night retrieval is run where the solar zenith angle is greater than 90° or at least two visible/near-IR channels do not convey valid information. Twilight conditions are defined by solar zenith angles between 80° and 90°, where the 3.7 μm channel is not used due to solar contamination.

2.3.15 Quality Control

The quality of the CC4CL algorithm is based on the output diagnostics of the OE retrieval.

- The number of iterations: Indicates if the retrieval has converged.
- A convergence test: CC4CL uses the change in the cost function between iterations to determine whether a retrieval has converged.
- Cost function: If the cost function is approximately equal to the number of measurements then the retrieval is thought to have fit the model well. In practice, any retrieval with cost greater than ten times the number of measurements is considered suspect.
- Error estimates: If the previous criteria is satisfied then the uncertainty on the retrieved parameters is given in the solution covariance.

2.4 Retrieval scheme performance

In this section we examine the theoretical performance of the cloud retrieval for a single-layer cloud when processing ATSR data as during the GRAPE project (described by Sayer et al. [2011] and Poulsen et al. [2012]). It investigates at what optical depths and effective radii the retrieval algorithm performs well for single-layer clouds.

2.4.1 Sensitivity study of single-layer cloud retrievals

Linear simulations are used to evaluate the sensitivity of observations to cloud parameters and error sources. The results are computed for a specific set of atmospheric profiles and observing conditions. Observation sensitivities are then transformed into retrieval sensitivity by assuming that the cloud forward model is linear within some suitable range about the atmospheric/observing state.

2.4.2 Simulation Setup

In addition to the conditions outlined in section 2.3, linear simulations were performed for:

- Solar zenith angle 30°, relative azimuth 0° and satellite zenith angle 0°;
- A standard temperature, humidity and trace-gas profile for northern mid-latitudes;
- Optical depths of 0.01, 0.5, 1, 3, 5, 7, 10, 12, 15, 20, 25, 30, 50 and 100 for liquid and ice clouds;

- Effective radii of 3, 5, 6, 7, 8, 9, 10, 12, 14, 16, 18, 20, 22 and 25 μm for liquid clouds and 3, 5, 8, 10, 12, 15, 20, 25, 30, 35, 40, 50 and 60 μm for ice clouds;
- An assumed sea surface;
- A fixed cloud fraction of 1.

Figure 3 shows the simulated retrieval uncertainties, i.e. the square root of the uncertainty covariance $\mathbf{S}_x$, as a percentage of the expected retrieved parameter for a single layer of ice or liquid cloud as a function of its optical depth and effective radius. (Note the differing radii ranges). The primary findings are:

- The percentage uncertainty on the optical depth increases as clouds become optically thick and is high for very optically thin clouds.
- For effective radius, the percentage uncertainty is largest for optically thin clouds and very small radii.
- The percentage uncertainty on the cloud top pressure is largest for very thin clouds.
- The percentage uncertainty for cloud liquid/ice path is greater for ice clouds and increases with optical depth and effective radius. It is also high for optically thin clouds.

From this simulation, it is clear that uncertainties are greater for clouds that are optically thin, extremely optically thick or have small effective radii. This simulation assumes that the optical models of the liquid and ice cloud are correct, such that the reported uncertainty will be an underestimate. Ice clouds are more difficult to model than water clouds due to the variation in type, i.e. hexagonal aggregates, rosettes, and the choice of optical model could have a significant effect on the accuracy of the retrieval [Zhang et al., 2009].

3 Input and output data

The primary input data used by CC4CL are calibrated, geolocated satellite radiances, generally referred to as level 1 data.

- When applied to (A)ATSR data, CC4CL ingests standard ESA level 1b data.
- NASA M*D021KM radiance and M*D03 geolocation files are the primary input for MODIS retrievals, where the "*" represents either an "O" for MODIS-TERRA or "Y" for MODIS-AQUA data.
- AVHRR data are ingested via the level 1 "avhrr" and "sunsatangles" files obtained from "pygac", which is a python package to read and calibrate NOAA AVHRR GAC data. It has been developed by SMHI (Swedish Meteorological and Hydrological Institute) as a standalone tool based on the precursor "AHAMAP", which was used in the PPS (Polar Platform System) 2010 CLARA-A1 processing in CMSAF. DWD (Deutscher Wetterdienst) has reprocessed AVHRR level 1 data using pygac in order to provide the required input for Cloud_cci.

The physical quantity measured by satellite radiometers is radiance. Two modifications are made to the radiance for use with CC4CL: the shortwave channels are scaled by the cosine of the solar zenith angle and normalised, to produce a sun-normalised reflectance, and the thermal channel radiances are converted to brightness temperatures in Kelvin.

These files then provide CC4CL with:

- Calibrated TOA reflectance/brightness temperature;

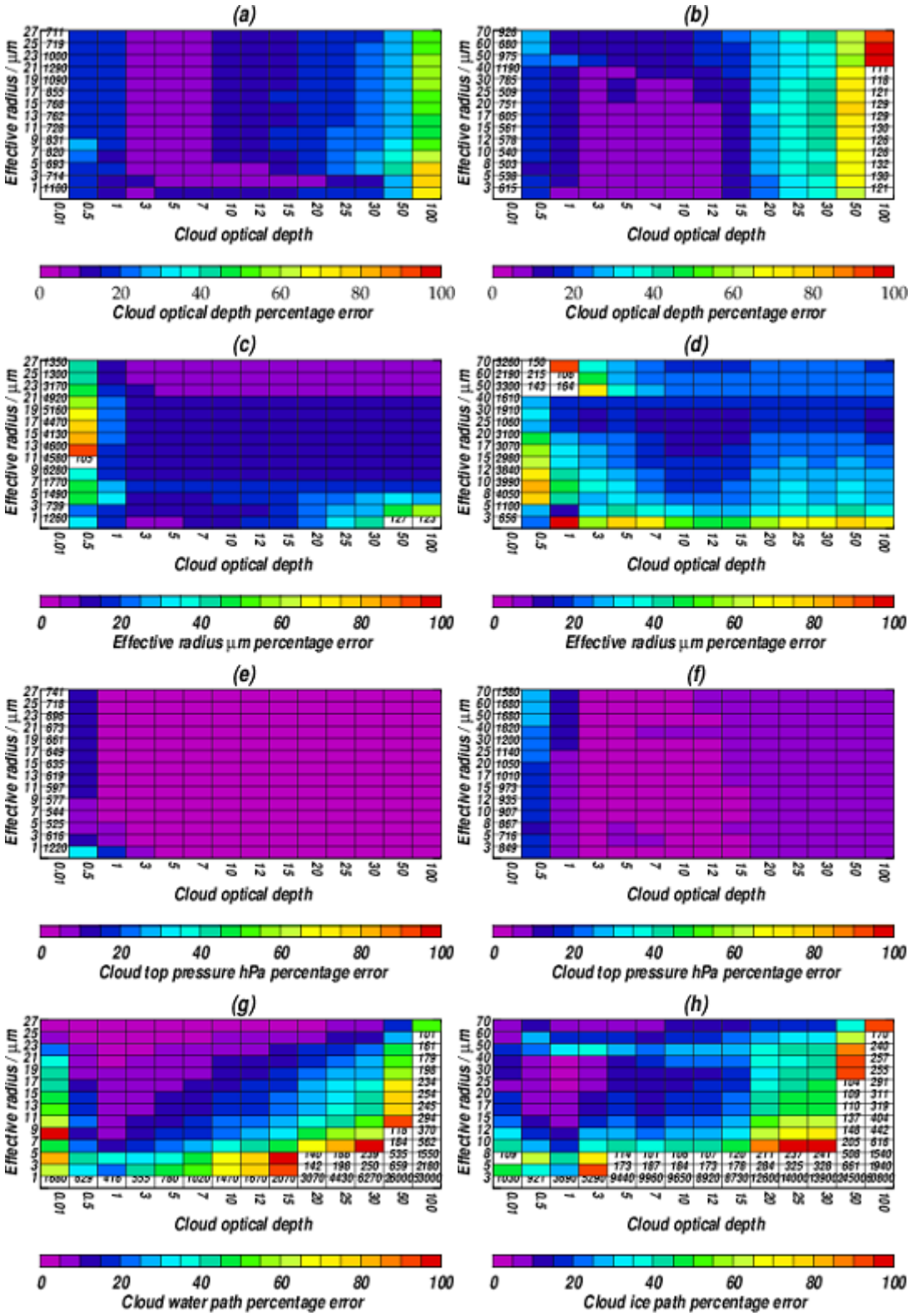

Figure 3: Simulated retrieval uncertainty as a function of varying effective radii and cloud optical depth for cloud optical depth (a) and (b), effective radius (c) and (d), cloud top pressure (e) and (f) and cloud liquid/ice path (g) and (h). Results for simulated liquid (left) and simulated ice (right) single layer cloud over sea.

- Solar and satellite azimuth and zenith angles;
- A land/sea mask for the level 1 grid.

CC4CL also makes use of a range of ancillary data:

- ECMWF ERA Interim humidity and temperature profiles, total column ozone, surface temperature and pressure, and 10 m east-west and north-south (u and v) wind components. These are used by the sea surface reflectance model to determine surface roughness and whitecap coverage and to estimate the sea surface emissivity.
- MODIS MCD43C1 surface BRDF product produced every 8 days with a 16-day acquisition from both Aqua and Terra-based MODIS observations [Lucht et al., 2000, Schaaf et al., 2002].
- The emissivity over land is taken from the CIMSS database [Seemann et al., 2007].
- SSMI snow and ice clouds masks [Nolin et al., 1998] are used to modify the surface albedo over the pole.

The parameters retrieved by CC4CL are constrained to the following ranges:

- The $\log_{10}$ of cloud optical depth at 0.55 μm: [-3 – 2.408]
- The effective radius (in μm): [0.1 – 35 (liquid) or 100 (ice)]
- The cloud top pressure (in hPa): [10 – 1200]
- Surface temperature (in K): [250 – 320]

In addition to the retrieved state parameters, a number of cloud variables are derived and stored in the global-level cloud products. Cloud top pressure is converted to cloud top height and temperature using the ECMWF temperature/pressure profiles. Cloud water path CWP is derived using the method of Han et al. [1994]

$$CWP = \frac{4}{3}\frac{\tau \cdot r_{\text{eff}} \cdot \rho}{Q_{ext}}, \tag{35}$$

where Q_{ext}, the extinction coefficient, is assumed to be 2 for water and 2.1 for ice for wavelengths much less than r_{eff}. The density ρ is $1\,\text{g}\,\text{m}^{-3}$ for water and $0.9167\,\text{g}\,\text{m}^{-3}$ for ice. Depending on phase, CWP is also known as liquid water path (LWP) or ice water path (IWP).

More technical descriptions of CC4CL's inputs, outputs, and data formats, in addition to example data files, can be found at the project's code repository at `http://proj.badc.rl.ac.uk/orac`.

Appendices

A Bayesian scene identification

Although not part of the operational CC4CL scheme used to produce the Phase I Cloud_cci products, the use of Bayesian statistics on the retrieval output to refine the cloud masking and phase selection – together described as scene identification – has been investigated. A brief description of the methodology and initial results is provided here.

A posteriori Bayesian scene identification is concerned with answering the question, "What is the probability that a given retrieval result is consistent with the measurements and our prior knowledge of the atmospheric state?" Given an answer to that question for a range of assumed cloud and/or aerosol properties, we can further ask whether the measurements provide a clear indication of which set of those assumptions best describes the observations.

As described in section 2, an OEM retrieval is constructed based on maximising the Bayesian probability of the retrieved state, conditional on the measurements and *a priori* constraints. This formulation assumes that the uncertainties in both the measurement and *a priori* are Gaussian and that the retrieval is nearly linear within the region defined by these uncertainties. Rodgers [2000] shows that the cost function $J(\vec{x})$ is directly related to this conditional probability through the expression

$$P(\vec{x}|\vec{y},\ \vec{x_{\mathrm{a}}}) = P(\vec{x_{\mathrm{a}}}) \exp\left(-\frac{J(\vec{x})}{2}\right). \tag{36}$$

It is clear, therefore, that a well-characterised optimal estimation retrieval scheme not only provides state estimates with fully propagated uncertainties but can also provide probabilistic measures of the consistency of the state with the measurement and *a priori*.

If we examine the expression for the OEM cost function:

$$J(\vec{x}) = [\vec{y}(\vec{x}) - \vec{y_{\mathrm{m}}}]\, \mathbf{S_y}^{-1}\, [\vec{y}(\vec{x}) - \vec{y_{\mathrm{m}}}]^T + (\vec{x} - \vec{x_{\mathrm{a}}})\, \mathbf{S_a}^{-1}\, (\vec{x} - \vec{x_{\mathrm{a}}})^T, \tag{37}$$

we can identify the two terms on the right hand side: the measurement cost J_{m} and the *a priori* cost J_{a}. In situations where the forward model is a good representation of the true atmosphere, in that it is able to reproduce the observed TOA radiances while remaining consistent with the prior constraints, these terms should represent random samples from normal distributions with differing degrees of freedom. J_{a} is the degrees of freedom equal the number of elements in the state vector. J_{m} is equal to the degrees for freedom of signal d_{s}, which is the number of independent pieces of information provided by the measurement above the level of noise and is defined by:

$$d_{\mathrm{s}} = \mathrm{tr}\left(\mathbf{K}\mathbf{S_a}\mathbf{K}^T \left[\mathbf{K}\mathbf{S_a}\mathbf{K}^T + \mathbf{S_y}\right]^{-1}\right), \tag{38}$$

where $\mathrm{tr}\,(\mathbf{A})$ denotes the trace of the matrix $\mathbf{A}$.

Thus, by comparing the cost function components to the χ^2 distribution — the distribution of the sum of the squares of a set of normally distributed random variables — with the appropriate degrees of freedom, we can calculate the probability that any given retrieval lies within the expected range described by the measurement and *a priori* uncertainties. This is the standard χ^2 test and provides the probabilistic measure of consistency for each retrieval. The test can be performed separately for both the measurement and *a priori* constraint and the resulting probabilities multiplied to produce an overall value, denoted by $\mathcal{P}$.

In the case where the cloud phase is ambiguous (see section 2.2), the $\mathcal{P}$ statistic can provide useful additional insight. Selecting the phase with the highest $\mathcal{P}$ value is equivalent to selecting that with the lowest cost, but in addition one can ascertain the following:

- The probability that each phase is the correct one, based on the measurement and *a priori* constraints. If no phase provides a result which is consistent with the measurement then the atmospheric state lies outside the range of assumptions made in the forward model and the results should be treated with caution.

- Under the assumption that only one phase can be the correct one, we assume that the one with the highest probability is the correct one. In general terms, if N phases have been tried in the retrieval, then the probability that the nth phase is the correct one can be written:

$$\mathcal{P}'_{\mathrm{n}} = \frac{\mathcal{P}_{\mathrm{n}}}{\sum_{i=1}^{N} \mathcal{P}_i}. \tag{39}$$

The question of phase discrimination can also be generalised to include cloud detection, through the inclusion of background aerosol types (such as maritime aerosol over the oceans) and episodic aerosols, such as desert dust, which might be detected as cloud by traditional threshold-based cloud flagging.

As the $\mathcal{P}$ statistic represents the Bayesian probability of a particular state being consistent with the measurements and prior constraints, within the framework of the retrieval forward model and uncertainty budget, it offers two key advantages:

1. The probability $\mathcal{P}$ represents the true constraint on the atmospheric state provided by the measurement, under the assumptions made in the retrieval. Cloud retrievals are generally under-constrained and a probability provides a intuitive and easily understood measure of the ambiguity of a retrieval result.

2. The availability of a probabilistic cloud mask and phase selection provides a quantitative method of combining the constraint provided by the retrieval itself with prior and posterior constraints through Bayesian methods.

The accuracy — in terms of the probability values produced — of this approach does require that the retrieval uncertainty budget be well understood. If measurement and forward modelling uncertainties are inaccurate, the resulting PDF of the retrieval cost function will not follow the χ^2 distribution and the values of $\mathcal{P}$ produced will be erroneous.

References

Baran, A. J. and Havemann, S., The dependence of retrieved cirrus ice-crystal effective dimension on assumed ice-crystal geometry and size-distribution function at solar wavelengths, Q. J. R. Meteorol. Soc., 130, 2153–2167, doi: 10.1256/qj.03.154, 2004.

Baran A. J., Shcherbakov V.N., Baker B. A., Gayet J. F. and Lawson RP., On the scattering phase function of non-symmetric ice crystals, Q. J. R. Meteor Soc., 131, 260916, 2005.

Birks, A., Improvements to the AATSR IPF relating to land surface temperature, ESA Technical note. AATSR Product Handbook, Issue 1.2, European Space Agency, 2004.

Cox, C. and Munk, W., Measurement of the roughness of the sea surface from photograhs on the Sun's glitter, J. Opt. Soc. Am., 44, 838–850, doi:10.1364/JOSA.44.000838, 1954.

Cox, C. and Munk, W., Statistics of the sea surface derived from Sun glitter, J. Mar. Res., 13, 198–227, 1954.

Dee, D. P., Uppala, S. M., Simmons, A. J., Berrisford, P., Poli, P., Kobayashi, S., Andrae, U., Balmaseda, M. A., Balsamo, G., Bauer, P., Bechtold, P., Beljaars, A. C. M., van de Berg, L., Bidlot, J., Bormann, N., Delsol, C., Dragani, R., Fuentes, M., Geer, A. J., Haimberger, L., Healy, S. B., Hersbach, H., Hlm, E. V., Isaksen, L., Kllberg, P., Khler, M., Matricardi, M., McNally, A. P., Monge-Sanz, B. M., Morcrette, J.-J., Park, B.-K., Peubey, C., de Rosnay, P., Tavolato, C., Thpaut, J.-N. and Vitart, F., The ERA-Interim reanalysis: configuration and performance of the data assimilation system, Q.J.R. Meteorol. Soc., 137, 553–597, doi:10.1002/qj.828, 2011.

Han, Q., Rossow, W. B. and Lasis, A. A., Near-Global Survey of Effective Droplet Radii in Liquid Water Clouds Using ISCCP Data, J. of Climate, 7, 465–497, 1994.

Koepke, P., Effective Reflectance of Oceanic Whitecaps, AO, 23, 1816–1824, doi:10.1364/AO.23.001816, 1984.

Lean, K., Empirical methods for detecting atmospheric aerosol events from satellite measurements, MPhys. Project Report, University of Oxford, `http://www.atm.ox.ac.uk/group/eodg/mphys_reports/2009_Lean.pdf`, 2009.

Levenberg, K., A method for the solution of certain nonlinear problems in least squares, Quart. Appl. Math., 2, 164–168, 1944.

Lucht, W., Schaaf, C.B., and Strahler, A.H., An Algorithm for the Retrieval of Albedo from Space Using Semiempirical BRDF Models, Atmospheric Science, Surface Radiative Properties/BRDFs, TGRS, 38, 977–998, doi:10.1109/36.841980, 2000.

Nolin, A., Armstrong, R. L. and Maslanik, J., Near-Real-Time SSM/I-SSMIS EASE-Grid Daily Global Ice Concentration and Snow Extent. Boulder, Colorado USA: National Snow and Ice Data Center, 1998.

Marquardt, D. W., An algorithm for least-squares estimation of nonlinear parameters, SIAM, J. Appl. Math., 11, 431–441, doi:10.2307/2098941, 1963.

Morel, A. and Prieur, L., Analysis of Variations in Ocean Color, Limnology and Oceanography, 22, 709–722, doi:10.4319/lo.1977.22.4.0709, 1977.

MTG Level 2 Processing Specification Document, Document Number EUM/MTG/SPE/12/1078, March 2014.

Pavolonis, M. J. and Heidinger A. K., Daytime Cloud Overlap Detection from AVHRR and VIIRS, J. Appl. Meteor., 43, 762–778, doi:10.1175/2099.1, 2004.

Pavolonis, M. J., Heidinger A. K., and Uttal, T., Daytime Global Cloud Typing from AVHRR and VIIRS: Algorithm Description, Validation, and Comparisons, J. Appl. Meteor., 44, 804-826, doi:10.1175/JAM2236.1, 2005.

Poulsen, C. A., Siddans, R., Thomas, G. E., Sayer, A. M., Grainger, R. G., Campmany, E., Dean, S. M., Arnold, C., and Watts, P. D., Cloud retrievals from satellite data using optimal estimation: evaluation and application to ATSR, Atmos. Meas. Tech., 5, 1889–1910, doi:10.5194/amt-5-1889-2012, 2012.

Rodgers, C. D., Inverse methods for atmospheric sounding: Theory and Practice. Series on Atmospheric, Oceanic and Planetary Physics, Vol. 2, World Scientific, 2000.

Saunders, R. W., Matricardi, M. and Brunel, P., An Improved Fast Radiative Transfer Model for Assimilation of Satellite Radiance Observations, Q. J. R. Meteor. Soc., 125, 1407–1425, 1999.

Sayer A. M, Poulsen, C. A., Arnold, C., Campmany, E., Dean, S., Ewen, G. B. L., Grainger, R. G., Lawrence, B. N., Siddans, R., Thomas, G. E., and Watts, P. D., Global retrieval of ATSR cloud parameters and evaluation (GRAPE): dataset assessment Atmos. Chem. Phys., 11, 3913–3936, doi:10.5194/acp-11-3913-2011, 2011.

Sayer, A. M., Thomas, G. E. and Grainger, R. G., A sea surface reflectance model for (A)ATSR, and application to aerosol retrievals, Atmos. Meas. Tech., 2010, 3, 813–838, 4, 2010

Schaaf, C. B., F. Gao, A. H. Strahler, W. Lucht, X. Li, T. Tsang, N. C. Strugnell, X. Zhang, Y. Jin, J.-P. Muller, P. Lewis, M. Barnsley, P. Hobson, M. Disney, G. Roberts, M. Dunderdale, C. Doll, R. d'Entremont, B. Hu, S. Liang, and J. L. Privette, and D. P. Roy., First Operational BRDF, Albedo and Nadir Reflectance Products from MODIS, Remote Sens. Environ., 83, 135–148, 2002.

Schaepman-Strub, G., Schaepman, M. E., Painter, T. H., Dangel, S., Martonchik J. V., Reflectance quantities in optical remote sensing — definitions and case studies., Remote Sens. Environ., 103, 27–42, 2006.

Seemann, S. W., Borbas, E. E., Knuteson, R. O., Stephenson, G. R. and Huang, H.-L. Development of a Global Infrared Land Surface Emissivity Database for Application to Clear Sky Sounding Retrievals from Multi-spectral Satellite Radiance Measurements., Appl. Meteor. Climatol., 47, 108–123, 2007.

R. Siddans, C. Poulsen, E. Carboni Cloud Model for Operational Retrievals from MSG SEVIRI Final Report DRAFT Version 1.0, Eumetsat Contract EUM/CO/07/4600000463/PDW, January 26, 2011

Sus, O., Jerg, M., Poulsen, C., Thomas, G., Stapelberg, S., McGarragh, G., Povey, A., Schlundt, C., Stengel, M., and Hollmann, R.: The Community Cloud retrieval for CLimate (CC4CL). Part I: A framework applied to multiple satellite imaging sensors, submitted to Atmospheric Measurement Techniques Discussions, pp. , 2017.

Stamnes K., Tsay S.C., Wiscombe W. and Jayaweera K., Numerically stable algorithm for discrete ordinate method radiative transfer in multiple scattering and emitting layered media., Appl. Opt., 12, 2502–2509, 1988.

Takano, Y., and Liou, K. N., Solar radiative transfer in cirrus clouds. Part I: Single-scattering and optical properties of hexagonal ice crystals., J. Atmos. Sci., 46, 3–19, 1989.

Thomas, G. E., Carboni, E., Sayer, A. M., Poulsen, C. A., Siddans, R. and Grainger, R. G., Oxford-RAL Aerosol and Cloud (ORAC): aerosol retrievals from satellite radiometers, in *Satellite aerosol remote sensing over land*, Kokhanovsky, A. A. and de Leeuw, G. (eds.), Springer-Praxis, 2009.

Wanner, W., Strahler, A. H., Hu, B., Lewis, P., Muller, J.-P., Li, X., Barker Schaaf, C. L., and Barnsley, M. J., Global Retrieval of Bidirectional Reflectance and Albedo Over Land from EOS MODIS and MISR Data: Theory and Algorithm, JGR, 102, D14, 17143–17161, doi:10.1029/96JD03295, 1997.

Watts, P. D., Mutlow, C. T., Baran, A. J. and Zavody, A. M., Study on cloud properties derived from Meteosat Second Generation Observations. Eumetsat Report, `http://www.eumetsat.int/Home/index.htm`, 1998

Zhang Z., Yang, P., Kattawar, G., Riedi, J., Labonnote, L. C.-, Baum, B. A., Platnick, S., and Huang, H.-L., Influence of ice particle model on satellite ice cloud retrieval: lessons learned from MODIS and POLDER cloud product comparison, Atmos. Chem. Phys., 9, 7115–7129, 2009.